Nonlinear Model Predicts Diverse Respiratory Patterns of Birdsong

Marcos A. Trevisan,[1] Gabriel B. Mindlin,[1,*] and Franz Goller[2]

[1]*Departamento de Física, FCEN, Universidad de Buenos Aires Ciudad Universitaria, Pab. I (1428) - Buenos Aires, Argentina*
[2]*Department of Biology, University of Utah, Salt Lake City, Utah 84112, USA*
(Received 29 April 2005; published 6 February 2006)

A central aspect of the motor control of birdsong production is the capacity to generate diverse respiratory rhythms, which determine the coarse temporal pattern of song. The neural mechanisms that underlie this diversity of respiratory gestures and the resulting acoustic syllables are largely unknown. We show that the respiratory patterns of the highly complex and variable temporal organization of song in the canary (Serinus canaria) can be generated as solutions of a simple model describing the integration between song control and respiratory centers. This example suggests that subharmonic behavior can play an important role in providing a complex variety of responses with minimal neural substrate.

The characteristic temporal patterns of birdsong, with alternating sound and silence, arise primarily from the activity of respiratory muscles [1]. Sound is typically generated during expiration as the elevated air pressure drives the airflow that induces phonation. Silent periods in between song elements correspond to short inspirations (minibreaths) unless the sound pulse rate is very high [2,3]. A remarkable capacity to rapidly switch between expiration and inspiration gives rise to the complex temporal song structure and at the same time allows birds to sing long, uninterrupted songs. Song in the Waterslager canary is a long sequence of distinct syllables, each of which is repeated a variable number of times (phrase) before a switch to a new syllable type occurs. Syllable repetition rate varies between phrase types and can be as high as 30 Hz for syllables that are followed by a minibreath and even greater than 60 Hz for phrases which are sung during a sustained expiration (pulsatile syllables) [4,5]. Song is a learned behavior, and it is unknown how the motor gestures for different syllable types, with remarkably different rhythms, are represented in the central motor program.

A song is built out of a diversity of syllables. Each syllable is generated by the vocal organ when activated by a specific pressure pattern. The different pressure patterns could be generated when the appropriate muscles are activated either by different neural populations, or by a unique neural population displaying a variety of activity patterns. The latter scenario is possible since neurons behave as nonlinear devices. Nonlinear systems are known to exhibit qualitatively different behaviors (with strict topological restrictions) under different parameters. Therefore, a variety of temporal patterns can be generated by a single system under different operational regimes. Here we use a variety of tools from nonlinear dynamics to show that the temporal features of air sac pressure data recorded from singing canaries can be reproduced with such a simple model.

The sonogram of the song depicted in Fig. 1 presents three regimes (A, B, and C) characterized by different syllable repetition rates. Simultaneous to the measurement of the song we recorded the air sac pressure [see methods (a)]. The pressure time series corresponding to the sonogram of Fig. 1 is displayed in Fig. 2(a). In this figure, we can notice that regimes B and C are different from regime A, since the pressure presents large fluctuations. Since each regime is generated by an almost periodic pressure pattern, we analyzed the pressure time series data with techniques developed in the field of nonlinear dynamics to study recurrent trajectories. We extracted segments of data corresponding to each regime, and embedded them in a three-dimensional phase space [see methods (b)] [6]. Then, we studied their topological organization in phase space [6]. Specifically, we computed the linking numbers between the extracted segments ([see methods (c)]. The purpose for this calculation is to provide a quantitative way to support a model. The linking numbers act as a fingerprint: if the orbits generated by a model fail to present the topological organization of the experiments, the model has to be rejected [6]. This procedure is analogous to standard tests (e.g., least squares) in linear systems [6,7]. The embedded segments of pressure data are displayed in Fig. 2(c). The segments extracted from regimes A and B do not link each other (they could be separated an arbitrary distance in the
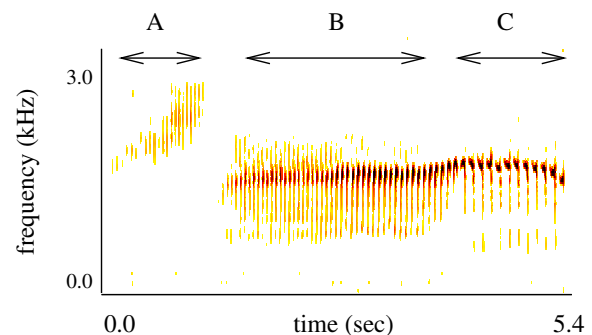

FIG. 1 (color online).　Acoustic identity of song syllables in canaries (spectrogram). Three different temporal patterns are identified in terms of the local spectral properties of the air sac pressure, denoted by A, B, and C.
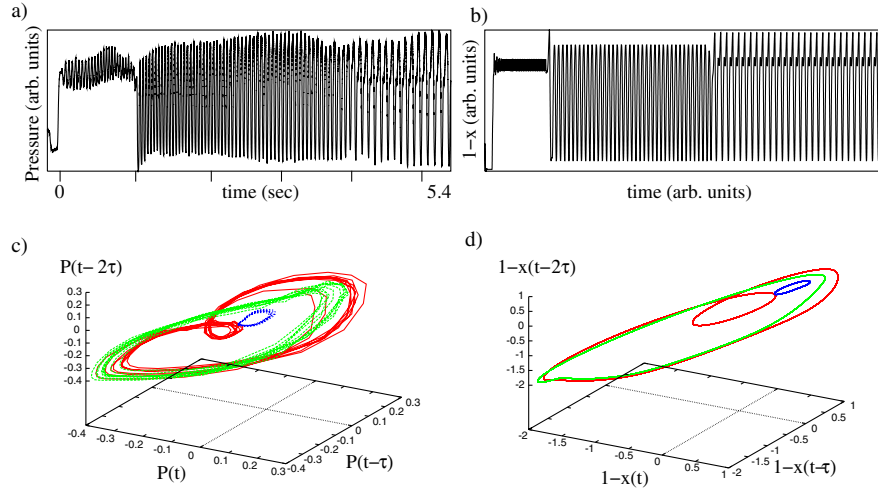
FIG. 2 (color online).   The recorded air sac pressure time series data contains 3 syllable types with different spectral characteristics (a). The entire respiratory pattern can be simulated by a periodically driven model by changing the forcing frequency twice in order to generate the three different segments. Equations were integrated with the following parameters: $m = 0.5$, $t = 1.0$, $k = 1.0$, $\mu = 5.0$, $E_1 = -1.3$, and $E_2 = -1.5$. (b) Embedded segments (with a time delay of 0.31 sec) can be used to characterize the data. Dotted (in online version, blue) segments correspond to type A patterns, dashed (in the online version, green) segments correspond to type B patterns, while the solid lines are used to plot the patterns of type C (in online version, red). (c) The embedding of the synthetic patterns allows a comparison between experimental data and model of topological nature. If the topological organization of the model does not match the data, the model is rejected (d). The topological organization can be described through indexes as the linking numbers between orbits.

embedding space without the orbits ever intersecting), while the segments of regime C link around the segments of regime B (i.e., they can not be separated an arbitrary distance in the embedding space without the orbits intersecting at some point).

We compared these features of the experimental data with synthetic pressure data generated by a computational model inspired in the known anatomy of oscine birds. As sketched in Fig. 3, we describe the air sac dynamics by a
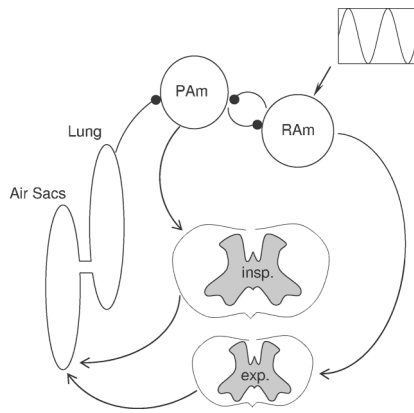

FIG. 3.   Schematic of the proposed organization for integration of central song control and respiratory centers. Inhibitory connections are indicated by a black circle. Abbreviations: Insp, inspiratory motor neurons; Exp., expiratory motor neurons. Arrows indicate excitations, circles inhibition. PAm and RAm represent the nuclei parambigualis and retroambigualis, respectively. The oscillatory input represents a basic oscillation generated by telencephalic nuclei.

variable x measuring the deviation from the volume of the sacs at atmospheric pressure. In Eq. (1a) we model the sacs as a damped mass (m), driven by inspiratory and expiratory muscles against mechanical restitution (restitution constant k), dissipation (dissipation constant μ). The activities of these muscles should be proportional to the activities of brainstem nuclei parambigualis PAm (i_1) and retroambigualis RAm (i_2), respectively [8,9], which are thought to be mutually inhibitory. These nuclei are the premotor nuclei for the spinal motor neurons controlling inspiration and expiration, respectively. Equations (1b) and (1c) describe the activity of these nuclei using one of the simplest neural additive models [10]. A harmonic function is used as a simple input in our model to emulate the oscillatory telencephalic activity triggering birdsong production [11,12].

A mathematical implementation (or computational model) of the integrated neural-mechanical system can be written as a dynamical system as this:

$$m\frac{d^2x}{dt^2} + kx + \mu\frac{dx}{dt} = 2i_1 - i_2 \tag{1a}$$

$$\tau\frac{di_1}{dt} = -i_1 + S[E_1 - i_2 - f(x)] \tag{1b}$$

$$\tau\frac{di_2}{dt} = -i_2 + S[E_2 - i_1 + A\cos(\varpi t)], \tag{1c}$$

where Eqs. (1b) and (1c) describe the way in which the activity of each nucleus converges either to zero (no activity) or to at most a saturation value, depending on the total input on the nucleus [the sigmoideal function $S(x) = 1/(1 + e^{-x})$ provides a frequently used model for saturat-

ing functions, and is chosen for simplicity]. A monotonically increasing function $f(x) = 9x^3/(1 + x^3)$ represents the inhibitory effect of volume [13] and CO_2 sensors on the activity of the neurons responsible for inspiration (which ceases if the volume of the sacs increase beyond some value). The negative signs with which the activities i_1 and i_2 enter in the arguments of the sigmoideal functions account for the mutual inhibition of RAm and PAm. The right-hand side of Eq. (1a) accounts for the active control of RAm and PAm of expiratory and inspiratory muscles, respectively, and the coefficients of i_1 and i_2 are chosen so that the dynamical system (1a)–(1c), before being forced (i.e., $A = 0$), presents excitability. In order to emulate regimes A, B, and C we changed the driving frequency (ω) without altering the driving amplitude A (notice that changes in both parameters can give rise to different pressure patterns, but the change in the frequency of the forcing is a necessary condition to synthetize patterns that correspond to the experimental ones). The resulting synthetic pressure patterns are obtained by plotting $P_0 - x$, since the air sac pressure will be inversely proportional to the variable measuring the air sac volume departure from rest (x) [see Fig. 2(c)]. Beyond the similarity with the measured patterns [Figs. 2(a) and 2(b)], the segments emulating the different regimes were embedded like the experimental ones, and their topological organization was found to be identical [Figs. 2(c) and 2(d)].

The different solutions exhibited by our model are subharmonic solutions, i.e., n-periodic solutions that repeat themselves after an integral multiple of the forcing period (n) [14]. For different values of the forcing amplitude and frequency, different solutions are found. The regions of the parameter space, for which solutions of the same period are obtained, are known in the field of nonlinear dynamics as *Arnold tongues,* and their relative organization in the frequency domain is very strict [15,16]. For our model, the regions of the parameter space where different solutions are found is displayed in Fig. 4(a). Notice that for simplicity we use a harmonic function to emulate RA activity, but any periodic function driving our system would present the same solutions [16].

In order to further test the hypothesis that the pressure patterns of different syllables could be the solutions of a unique, simple systems driven at different parameter values, we classified the different pressure patterns recorded in different birds, according to their spectral content. In the three regimes present in the example (Fig. 1), we find the following spectral features [Fig. 4(a)]. The first regime presents a peak at about 25 Hz (left panel). The air sac pressure in regime B can be characterized by a large peak at 20 Hz (center panel), which slowly drifts toward smaller frequency values, even if acoustically, the syllables at the beginning and at the end of regime B present different features. Regime C presents two large peaks: one at 23 Hz, and a second one at 11.5 Hz (right panel). There are two competing explanations for this transition. Either the bird changes dramatically the fundamental frequency f_0 from
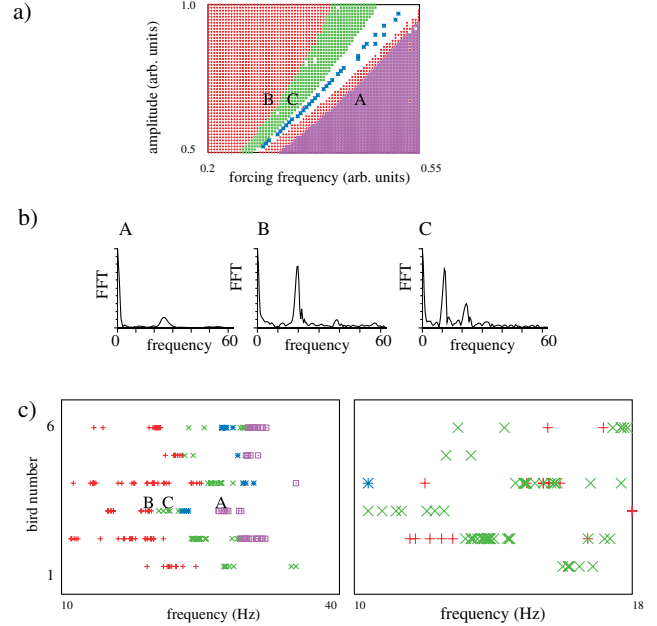

FIG. 4 (color). Arnold tongues for the model, displaying the regions of parameter space where different subharmonic solutions are found. The parameter values marked as A, B, and C were used to generate the synthetic emulating the pressure pattern of Fig. 2(a) (a). The spectral properties of the segments A, B, and C (b). A quantitative-qualitative classification scheme for pressure patterns generating different syllables for six birds. A, B, and C refer to the patterns in Figs. 1 and 2(a). The colors represent spectral features: red for large-amplitude solutions locked to the forcing frequency, green for period 2 solutions of large amplitude, blue corresponds to period 3 solutions, and pink for high frequency solutions mounted on a dc value (pulsatile syllables). The fundamental frequency of the segment is represented on the horizontal axis [(c), left]. The delicate structure shown in the left panel disappears under the hypothesis that the lower frequency in the fast Fourier transform of each solution is the fundamental one. A enlarged region from (10 to 18 Hz) displays a mixing of different pattern types under this assumption [(c), right].

regime B ($f_0 \sim 20$ Hz) to regime C ($f_0 \sim 11.5$ Hz) in a transition that also involves an important change of harmonics for the pressure pattern, or the bird makes a small change of the fundamental frequency (from $f_0 \sim 20$ Hz to $f_0 \sim 23$ Hz), and a classical bifurcation (period doubling) takes place, as in the model. If different patterns occur as the result of bifurcations, their fundamental frequencies would be organized in clusters ordered in specific ways, and spectral contents mostly concentrated in n peaks, the greatest of which would be identified as the fundamental frequency.

In the left panel of Fig. 4(c) we represent each syllable as a point, with its color representing the syllable type, located at the corresponding fundamental frequency (according to the bifurcation paradigm) of the air sac pressure pattern. Remarkably, the different syllable types present a clustered nature. For example, for each bird, the period 2 solutions are always found in between the solutions of

period 1 corresponding to trills (e.g., A in Fig. 1), and solutions of period 1 associated with large oscillations (B in Fig. 1). Also, solutions of type A occur, for each bird, at higher frequencies than those of type B. The solutions of period 3 are located, for each bird, at higher frequencies than those of large-amplitude period 1 solutions (e.g., regime B) and at lower frequencies than the solutions of regime A.

In the right panel of Fig. 4(c) we classify the pressure patterns according to the more parsimonious hypothesis that the lowest peak of the spectrum corresponds to the fundamental frequency. The bird would be capable of generating pressure patterns with the same fundamental frequency but completely different spectra of harmonics. Moreover, the delicate structure shown in the left panel [i.e., well-defined Arnold tongues, ordered relative to each other as predicted the theory of nonlinear dynamical systems [14,15,17]] disappears as solutions qualitatively different spectrally get mixed.

This work shows that the high diversity and complexity of respiratory patterns of canary song can emerge as different solutions of a simple system. It is notable that the remarkably different respiratory patterns of phrases involving minibreaths and pulsatile syllables arise from this model without a requirement for adding complexity. According to these findings, generation of diverse pressure patterns requires a system driven by different frequencies. Direct support for this neural model requires simultaneous measurement of activity in a telencephalic nucleus (as RA), and in the respiratory circuit (as in RAm). Because in many bird species the principal respiratory mechanisms of song production are similar to those of the canary, this model should be broadly applicable to singing behavior. Furthermore, the model identifies a possible neural mechanism for generating diverse rhythmic behavioral patterns in general, despite the differences between systems in their specific neural arrangements. Complex physiological rhythms in intact animals are poorly understood [17], but nonlinear mechanisms are beginning to be recognized as an important component of neural pattern generation [18]. The present example suggests that subharmonic behavior can play an important role in providing a complex variety of responses with minimal neural substrate.

Methods.—(a) The technique for measuring air sac pressure has been described in detail elsewhere [2–5]. Briefly, air sac pressure was registered by the insertion of a silastic cannula through the abdominal wall just posterior to the last rib, so that it extended a few millimeters into a thoracic air sac. The free end of the cannula was connected to a miniature piezoresistive pressure transducer (Fujikura model FPM-02PG), which was mounted on the bird's back. From this backpack the signals were transmitted to a signal conditioning unit (Hector Engineering) outside the cage, and the amplified signal was recorded simultaneously with microphone recordings (Audiotechnica AT8356) of the song on a multichannel data recorder

(TEAC RD-135T). We recorded several minutes of song from 6 male canaries, capturing most of the vocal repertoire of each male. (b) The construction of a multivariable environment for data (embedding) is performed by choosing the first coordinate of a three-dimensional vector as the variable at time t, the second and third as the recorded variable at time $t-\tau$, and $t-2\tau$, i.e., $(x(t), x(t-\tau), x(t-2\tau))$. The parameter τ is called delay, and the topology of a system is robust under this parameter [6]. (c) Gauss defined the linking number of two loops A and B, described by two vectors x_A and x_B [6] each of three components, as

$$L(\mathrm{A}, \mathrm{B}) = \iint (x_\mathrm{A} - x_\mathrm{B})(dx_\mathrm{A} \times dx_\mathrm{B})/|x_\mathrm{A} - x_\mathrm{B}|^3.$$

In order to compute the linking number between segments of data, we first built a vector of three components for each segment as described in (b), using a time delay of 0.31 sec. For each pair of segments, we used these vectors to calculate the Gauss integral. If A, B, and C represent loops in regimes A, B, and C of Fig. 1, we get $L(\mathrm{A}, \mathrm{B}) = 0$, $L(\mathrm{A}, \mathrm{C}) = 0$, $L(\mathrm{B}, \mathrm{C}) = 1$.

*Corresponding author.
[1] M. Konishi, Curr. Opin. Neurobiol. **4**, 827 (1994).
[2] R. Suthers, J. Neurobiol. **33**, 632 (1997).
[3] R. A. Suthers, F. Goller, and C. Pytte, Phil. Trans. R. Soc. B **354**, 927 (1999).
[4] R. S. Hartley and R. A. Suthers, J. Comp. Physiol. A **165**, 15 (1989).
[5] R. S. Hartley, Respiration Physiology **81**, 177 (1990).
[6] R. Gilmore and M. Lefranc, *The Topology of Chaos* (Wiley, New York, 2003).
[7] H. D. I. A. Abarbanel, *Analysis of Observed Chaotic Data* (Springer, New York, 1996).
[8] J. M. Wild, Ann. N.Y. Acad. Sci. **1016**, 438 (2004).
[9] C. B. Sturdy, J. M. Wild, and R. Mooney, J. Neurosci. **23**, 1072 (2003).
[10] F. C. Hoppensteadt and E. M. Izhikevich, *Weakly Connected Neural Networks* (Springer-Verlag, Berlin, 1997).
[11] H. R. Hahnloser, A. A. Kozhevnikov, and M. S. Fee, Nature (London) **419**, 65 (2002).
[12] A. C. Yu and D. Margoliash, Science **273**, 1871 (1996).
[13] J. Keener and J. Sneyd *Mathematical Physiology* (Springer, New York, 1998).
[14] H. G. Solari, M. A. Natiello, and G. B. Mindlin, *Nonlinear Dynamics: A Two Way Trip from Physics to Math* (IOP, London, 1996).
[15] M. Feingold, D. L. Gonzalez, O. Piro, and H. Viturro, Phys. Rev. A **37**, R4060 (1988).
[16] D. L. Gonzalez and O. Piro, Phys. Rev. Lett. **50**, 870 (1983).
[17] L. Glass, Nature (London) **410**, 277 (2001).
[18] M. S. Golubitsky, I. Stewart, Pietro-Luciano Buono, and J. J. Collins, Nature (London) **401**, 693 (1999).